Probing the pairing symmetry in the over-doped Fe-based superconductor $Ba_{0.35}Rb_{0.65}Fe_2As_2$ as a function of hydrostatic pressure

Z. Guguchia,[1,*] R. Khasanov,[1] Z. Bukowski,[2] F. von Rohr,[3] M. Medarde,[4]
P. K. Biswas,[1] H. Luetkens,[1] A. Amato,[1] and E. Morenzoni[1]

[1]*Laboratory for Muon Spin Spectroscopy, Paul Scherrer Institute, CH-5232 Villigen PSI, Switzerland*
[2]*Institute of Low Temperature and Structure Research, Polish Academy of Sciences, 50-422 Wroclaw, Poland*
[3]*Physik-Institut der Universität Zürich, Winterthurerstrasse 190, CH-8057 Zürich, Switzerland*
[4]*Laboratory for Developments and Methods, Paul Scherrer Institute, CH-5232 Villigen PSI, Switzerland*

(Received 14 October 2015; revised manuscript received 29 January 2016; published 11 March 2016)

We report muon spin rotation experiments on the magnetic penetration depth λ and the temperature dependence of λ^{-2} in the over-doped Fe-based high-temperature superconductor (Fe-HTS) $Ba_{1-x}Rb_xFe_2As_2$ ($x = 0.65$) studied at ambient and under hydrostatic pressures up to $p = 2.3$ GPa. We find that in this system $\lambda^{-2}(T)$ is best described by d-wave scenario. This is in contrast to the case of the optimally doped $x = 0.35$ system which is known to be a nodeless s^{+-}-wave superconductor. This suggests that the doping induces the change of the pairing symmetry from s^{+-} to d wave in $Ba_{1-x}Rb_xFe_2As_2$. In addition, we find that the d-wave order parameter is robust against pressure, suggesting that d is the common and dominant pairing symmetry in over-doped $Ba_{1-x}Rb_xFe_2As_2$. Application of pressure of $p = 2.3$ GPa causes a decrease of $\lambda(0)$ by less than 5%, while at optimal doping $x = 0.35$ a significant decrease of $\lambda(0)$ was reported. The superconducting transition temperature T_c as well as the gap to T_c ratio $2\Delta/k_BT_c$ show only a modest decrease with pressure. By combining the present data with those previously obtained for optimally doped system $x = 0.35$ and for the end member $x = 1$, we conclude that the SC gap symmetry as well as the pressure effects on the SC quantities strongly depend on the Rb doping level. These results are discussed in the light of the putative Lifshitz transition, i.e., a disappearance of the electron pockets in the Fermi surface of $Ba_{1-x}Rb_xFe_2As_2$ upon hole doping.

DOI: 10.1103/PhysRevB.93.094513

I. INTRODUCTION

The family of unconventional superconductors has grown considerably over the last couple of decades and now includes cuprates [1], heavy fermions [2], organic superconductors [3], and most recently iron pnictides [4,5]. They all share a similar phase diagram [6,7]. Superconductivity emerges through doping or applied pressure when the competing magnetic state is suppressed. Even after more than 20 years of intensive research the superconducting (SC) pairing mechanism is still not understood for the above mentioned compounds [8]. To understand it, it is instructive to study the symmetry and structure of the SC gap. A significant experimental and theoretical effort has concentrated on studies of this issue in Fe-HTS's. However, there is no consensus on a universal gap structure and the relevance for the particular gap symmetry for high-temperature superconductivity in iron-based high temperature superconductors (Fe-HTS's), which are the first noncuprate materials exhibiting superconductivity at relatively high temperatures. In contrast to cuprates, where the SC gap symmetry is universal the gap symmetry and/or structure of the Fe-HTS's can be quite different from material to material. For instance, nodeless isotropic gap distributions were observed in optimally doped $Ba_{1-x}K_xFe_2As_2$, $Ba_{1-x}Rb_xFe_2As_2$, and $BaFe_{2-x}Ni_xAs_2$ as well as in $BaFe_{2-x}Co_xAs_2$, $K_xFe_{2-y}Se_2$, and $FeTe_{1-x}Se_x$ [9–16]. Signatures of nodal SC gaps were reported in LaOFeP, LiFeP, KFe_2As_2, $BaFe2(As_{1-x}P_x)_2$, $BaFe_{2-x}Ru_xAs_2$ as well as in over-doped $Ba_{1-x}K_xFe_2As_2$ and $BaFe_{2-x}Ni_xAs_2$ [15,17–25].

We note that an important feature of $Ba_{1-x}Rb_xFe_2As_2$ and the related system $Ba_{1-x}K_xFe_2As_2$ is that the SC phase exists over a wide range of Rb and K concentration, respectively, namely from $x = 0.2$ to $x = 1$. For clarity, the schematic phase diagram for $Ba_{1-x}Rb_xFe_2As_2$ taken from Ref. [26] is shown in Fig. 1. The data points obtained in the present paper are also shown. It was found that this phase diagram is very similar to the thoroughly studied system $Ba_{1-x}K_xFe_2As_2$ [26]. The particularly interesting observation in $Ba_{1-x}K_xFe_2As_2$ is the systematic doping evolution of the nodal structure for heavy hole doping [27,28]. At around optimal doping $x = 0.4$, where T_c has a maximum value of 38 K, many experiments revealed the occurrence of multiple isotropic SC gaps. A sign changing s-wave state which is mediated by spin fluctuations has been invoked to explain some of the experimental results. However, this state is expected to be very fragile to the presence of nonmagnetic impurities, while Fe-HTS's are experimentally known to be robust against nonmagnetic impurities. A no-sign changing s_{++} wave state mediated by orbital fluctuations and which is robust against nonmagnetic impurities is another possible candidate for the pairing in this system. Hence, the SC pairing symmetry in the optimum region is still an open question. However, there is consensus that the SC gap structure itself is fully gapped for optimally doped samples of $Ba_{1-x}K_xFe_2As_2$. It is interesting that in this system, the crossover from nodeless to nodal SC state occurs at $x \sim 0.8$. These changes were related to a Lifshitz transition, reflecting the disappearance of the electron pockets in the Fermi surface (FS), at similar K-doping levels [28] (unlike optimally doped $Ba_{0.6}K_{0.4}Fe_2As_2$ which has both electron and hole FSs, only hole FSs were found in the extremely hole-doped KFe_2As_2 [29]). The nodeless SC gaps

*zurab.guguchia@psi.ch

 ©2016 American Physical Society

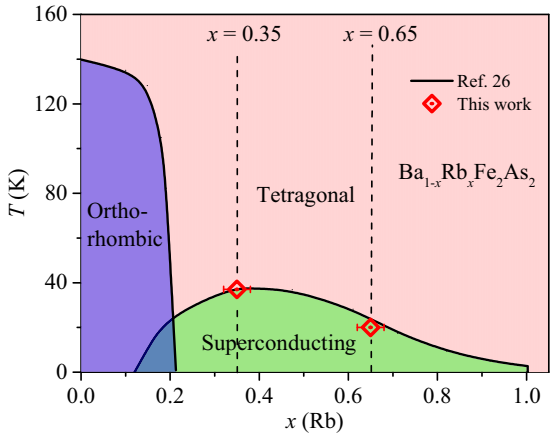

FIG. 1. Schematic phase diagram of $Ba_{1-x}Rb_xFe_2As_2$ (after Ref. [26]). The open symbols represent the values of the SC transition temperature obtained in this paper. The dashed lines mark the doping levels for our samples.

were also observed in $Ba_{1-x}Rb_xFe_2As_2$ at optimal doping $x = 0.3$, 0.35, 0.4 from the temperature dependence of the magnetic penetration depth λ by means of muon-spin rotation (μSR) [11]. μSR experiments performed on polycrystalline samples of extremely hole-doped $RbFe_2As_2$ also suggested the presence of two isotropic s-wave gaps [30,31]. However, recent specific heat and thermal conductivity measurements on single crystals of $RbFe_2As_2$ and on the related compound $CsFe_2As_2$ provided evidence for nodal SC gap in these materials [32–34]. This suggests that the crossover from nodeless to nodal state upon hole doping should also be present in $Ba_{1-x}Rb_xFe_2As_2$. In this regard it is important to study the SC gap symmetry in over-doped $Ba_{1-x}Rb_xFe_2As_2$.

Besides doping another important tuning parameter is the hydrostatic pressure which leads to new and in some materials very exotic physical properties, pressure induced phase transitions as well as changes of the characteristic SC or magnetic quantities [35–40]. In KFe_2As_2, a change of the SC pairing symmetry by hydrostatic pressure has been proposed, based on the V-shaped pressure dependence of T_c [38]. Recently, we have shown unambiguous evidence for the appearance of SC nodes in optimally-doped $Ba_{1-x}Rb_xFe_2As_2$ upon applied pressure, consistent with a change from a nodeless s^{+-}-wave state to a d-wave state [39]. Interestingly, the theoretical calculations [41–47] as well as Raman experiments [48,49] revealed a subdominant d-wave state close in energy to the dominant s^{+-} state. It seems that pressure affects this intricate balance and tips the balance in favor of the d-wave state. Besides the appearance of nodes with pressure in optimally-doped $Ba_{1-x}Rb_xFe_2As_2$, another interesting observation was a strong decrease of the magnetic penetration depth λ with pressure [39]. In contrast, in the end member compound $RbFe_2As_2$ an increase of λ and no change of the gap symmetry was found up to $p = 1.1$ GPa [31]. Thus, it is important to study the pressure effects on the SC properties of over-doped $Ba_{1-x}Rb_xFe_2As_2$ system in order to have a picture about the pressure effects on different regions of the phase diagram.

In the following we report on μSR studies of the temperature dependence of the penetration depth λ in over-doped $Ba_{0.35}Rb_{0.65}Fe_2As_2$ at ambient and under hydrostatic pressures up to $p = 2.3$ GPa. These results suggest the d-wave superconductivity in this system, which is distinctly different from the nodeless gap found at optimal doping. The d-wave order parameter symmetry is preserved under pressure. The SC transition temperature T_c, the value of the d-wave gap as well as the zero-temperature value of the magnetic penetration depth $\lambda(0)$ show only a modest decrease with pressure. We compare the present pressure data with the previous results of optimally doped $Ba_{0.65}Rb_{0.35}Fe_2As_2$ [39] and the end member $RbFe_2As_2$ [31] and discuss the combined results in the light of the possible Lifshitz transition in $Ba_{1-x}Rb_xFe_2As_2$ induced by hole doping.

II. EXPERIMENTAL DETAILS

Polycrystalline samples of $Ba_{1-x}Rb_xFe_2As_2$ ($x = 0.35$, 0.65) were prepared in evacuated quartz ampoules by a solid state reaction method. Fe_2As, BaAs, and RbAs were obtained by reacting high purity As (99.999%), Fe (99.9%), Ba (99.9%), and Rb (99.95%) at 800 °C, 650 °C, and 500 °C, respectively. Using stoichiometric amounts of BaAs or RbAs and Fe_2As the terminal compounds $BaFe_2As_2$ and $RbFe_2As_2$ were synthesized at 950 °C and 650 °C, respectively. Finally, the samples of $Ba_{1-x}Rb_xFe_2As_2$ with $x = 0.35$, 0.65 were prepared from appropriate amounts of single-phase $BaFe_2As_2$ and $RbFe_2As_2$. The components were mixed, pressed into pellets, placed into alumina crucibles, and annealed for 100 hours at 650 °C with one intermittent grinding. Magnetization, specific heat, powder x-ray diffraction, and μSR experiments were performed on samples from the same batch. This allows us to study the SC properties and the pressure effects in similar samples and to make direct comparison between the various properties in optimally and over-doped $Ba_{1-x}Rb_xFe_2As_2$. Powder x-ray diffraction analysis revealed that the synthesized samples are single phase materials. The magnetization measurements were performed with a commercial SQUID magnetometer (*Quantum Design* MPMS-XL). The specific heat measurements (relaxor type calorimeter Physical Properties Measurements System *Quantum Design*) were performed in zero field. Zero-field (ZF) and transverse-field (TF) μSR experiments were performed at the πM3 beamline of the Paul Scherrer Institute (Villigen, Switzerland), using the general purpose instrument (GPS). The sample was mounted inside of a gas-flow ^{4}He cryostat on a sample holder with a standard veto setup providing essentially a background free μSR signal. μSR experiments under various applied pressures were performed at the μE1 beamline of PSI, using the dedicated GPD spectrometer. Pressures up to 2.3 GPa were generated in a double wall piston-cylinder type of cell made out of MP35N material, especially designed to perform μSR experiments under pressure [50]. As a pressure transmitting medium Daphne oil was used. The pressure was measured by tracking the SC transition of a very small indium plate by AC susceptibility. All TF experiments were carried out after a field-cooling procedure. The μSR time spectra were analyzed using the free software package MUSRFIT [51].

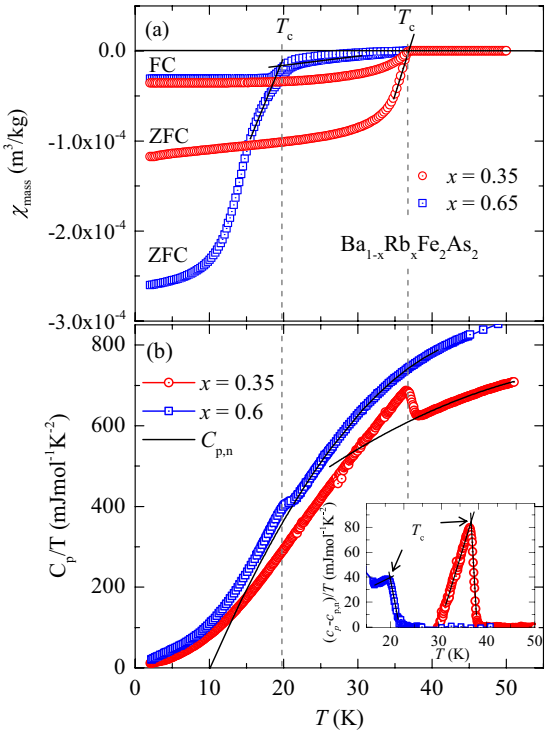

FIG. 2. Temperature dependence of the zero-field cooled (ZFC) and field-cooled (FC) susceptibility obtained in an applied magnetic field of $\mu_0 H = 2$ mT for $Ba_{1-x}Rb_xFe_2As_2$ ($x = 0.35, 0.65$). (b) The specific heat C_p/T as a function of temperature for $Ba_{1-x}Rb_xFe_2As_2$ ($x = 0.35, 0.65$). The dashed lines denote the superconducting transition temperatures T_c for both samples. The solid line is the fitted normal state contribution C_{pn}. The inset shows the specific heat with C_{pn} subtracted for different values of x.

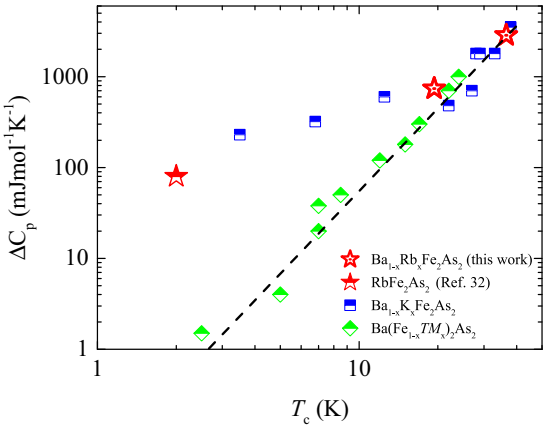

FIG. 3. ΔC_p at the superconducting transition vs T_c for $Ba_{1-x}Rb_xFe_2As_2$ ($x = 0.35, 0.65$), plotted together with literature data for some Fe-based SC materials, belonging to so-called '122' family (after Ref. [53]). The data point for $x = 0.35$ is taken from Ref. [39]. The line corresponds to $\Delta C_p \propto T^3$.

III. RESULTS AND DISCUSSION

A. Magnetization and specific heat capacity experiments

The temperature dependence of zero field-cooled (ZFC) and field-cooled (FC) diamagnetic susceptibility measured in a magnetic field of $\mu_0 H = 1$ mT for $Ba_{1-x}Rb_xFe_2As_2$ ($x = 0.35$, 0.65) is shown in Fig. 2(a). The SC transition temperature T_c for $x = 0.35$ is determined from the intercept of the linearly extrapolated zero-field cooled (ZFC) magnetization curve with $\chi_{mass} = 0$ line, and it is found to be $T_c = 37$ K. For the sample $x = 0.6$, $T_c = 20$ K was found, using the intercept of linear extrapolations above and below T_c, due to a small fraction with higher T_c. Temperature-dependent heat capacity data for both samples plotted as C_p/T vs T are shown in Fig. 2(b). The jumps associated with the SC transitions are clearly seen for both concentrations. The observed strong diamagnetic response and the specific heat jumps at T_c provide solid evidence for bulk superconductivity in both compounds. To quantify the jump in specific heat, the anomaly at the transition has been isolated from the phonon dominated background by subtracting a second order polynomial $C_{p,n}$ fitted above T_c and extrapolated to lower temperature [52]. The quantity $(C_p - C_{p,n})/T$ is presented as a function of temperature in the inset of Fig. 2(b). Although there is some uncertainty in using this procedure over an extended temperature range, the lack of appreciable thermal SC fluctuations, as evidenced by the mean-field-like form of the anomaly, means that there is very little uncertainty in the size of ΔC_p. It is evident from the inset of Fig. 2(b) that the size of the anomaly $\Delta C_p/T_c$ depends very strongly on x and T_c. A strong increase in ΔC_p with T_c has been observed previously in many '122' Fe-HTS's [53–55]. Bud'ko *et al.* found that in many '122' Fe-HTS's the specific heat jump ΔC_p at T_c follow the empirical trend, the so-called BNC scaling [53–55] $\Delta C_p \propto T^3$. This has been interpreted as either originating from quantum critically or from strong impurity pair breaking. A violation of the BNC scaling was observed for $Ba_{1-x}K_xFe_2As_2$ with $x > 0.7$, for which a change of the SC gap symmetry/structure was found [54,55]. The specific heat jump data for the $Ba_{1-x}Rb_xFe_2As_2$ samples obtained in this paper and one for the end member $RbFe_2As_2$ [32] are added in Fig. 3, to the BNC plot taken from Ref. [55]. The point for the optimally doped sample lies perfectly on the BNC line. On the other hand, the data point for $x = 0.65$ sample is slightly off from it and the point for the end-compound $RbFe_2As_2$ clearly deviates from this scaling. This indicates that the heavily over-doped $Ba_{1-x}Rb_xFe_2As_2$ shows a deviation from the BNC scaling, similar to that observed in related $Ba_{1-x}K_xFe_2As_2$. Hence, one expects significant changes in the nature of the SC state in the over-doped $Ba_{1-x}Rb_xFe_2As_2$.

B. μSR experiments

1. *Zero-field and transverse-field* μSR *on* $Ba_{0.65}Rb_{0.35}Fe_2As_2$ *and* $Ba_{0.35}Rb_{0.65}Fe_2As_2$ *at ambient pressure*

It is well known that undoped $BaFe_2As_2$ is not superconducting at ambient pressure and undergoes a spin-density wave (SDW) transition of the Fe moments far above T_c [56]. The SC state can be achieved either under pressure [57,58] or by appropriate charge carrier doping [59] of the parent compounds, leading to a suppression of the SDW state. Our first task was to check whether magnetism is present in the samples. Therefore, we have carried out ZF-μSR experiments above and below T_c in $Ba_{0.65}Rb_{0.35}Fe_2As_2$ and $Ba_{0.35}Rb_{0.65}Fe_2As_2$. As an example ZF-$\mu$SR spectra obtained above and below T_c are shown in Figs. 4(a) and 4(b), respectively. There are no precession

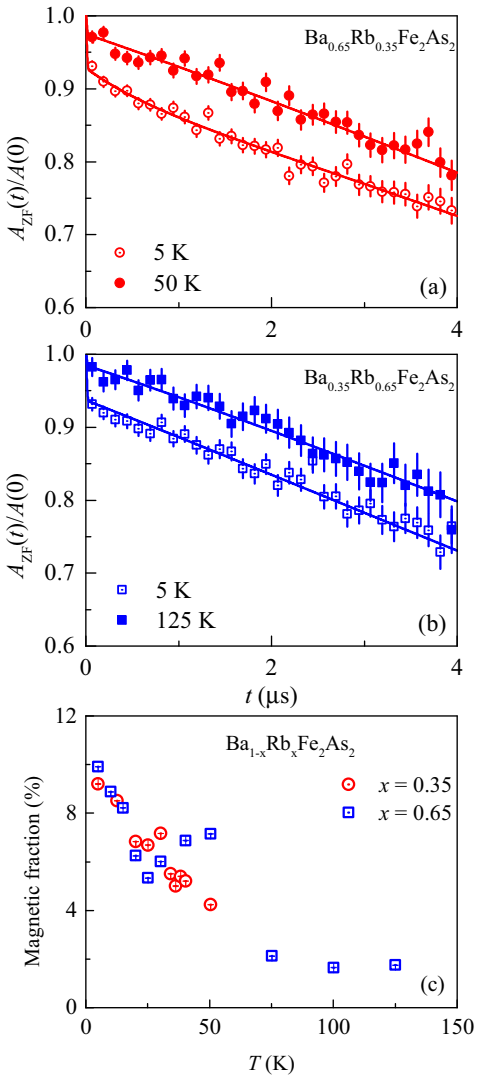

FIG. 4. ZF-μSR time spectra for $Ba_{0.65}Rb_{0.35}Fe_2As_2$ (a) and $Ba_{0.35}Rb_{0.65}Fe_2As_2$ (b) recorded above and below T_c. The line represents the fit to the data by means of Eq. (1). (c) Temperature dependence of the magnetic fraction in $Ba_{0.65}Rb_{0.35}Fe_2As_2$ and $Ba_{0.35}Rb_{0.65}Fe_2As_2$, extracted from the ZF-$\mu$SR experiments. The error bars represent the s.d. of the fit parameters, and they are smaller than the symbols.

signals, indicating the absence of long-range magnetic order. On the other hand, we observed a significant drop of the asymmetry, taking place within 0.2 μs. This is caused by the presence of diluted Fe moments as discussed in previous μSR studies [60]. In order to check the size of the magnetic fraction, the ZF-μSR data were analyzed by the following function:

$$A_{ZF}(t) = V_m A_0\left[\tfrac{1}{3}e^{-\lambda_L t} + \tfrac{2}{3}e^{-\lambda_T t}\right] + (1 - V_m)A_0 \times \left[\tfrac{1}{3} + \tfrac{2}{3}(1 - \sigma^2 t^2 - \Lambda t)e^{(-\frac{\sigma^2 t^2}{2} - \Lambda t)}\right]. \quad (1)$$

Here, the first and the second terms describe the magnetic and nonmagnetic parts of the signals, respectively. A_0 is the initial asymmetry, V_m is the magnetic volume fraction, and the λ_T, λ_L are the transverse and longitudinal depolarization rates of the μSR signal, respectively, arising from the magnetic part of the sample. The second term describing the paramagnetic part of the sample is the combination of Lorentzian and Gaussian Kubo-Toyabe depolarization function [61,62]. The depolarization rates σ and Λ are due to the nuclear dipole moments and randomly oriented diluted local electronic moments, respectively. The magnetic fraction obtained by fitting Eq. (1) to the data for $Ba_{0.65}Rb_{0.35}Fe_2As_2$ and $Ba_{0.35}Rb_{0.65}Fe_2As_2$ is plotted in Fig. 4(c). The magnetic fraction V_m was found to be only 10% in both samples at low temperatures. It decreases upon increasing the temperature and becomes negligibly small at around 80 K. By using Eq. (1) to extract the magnetic fraction we assume that the static magnetic order causes the initial loss of asymmetry. If the loss of asymmetry is caused by dynamic magnetism, than the estimated magnetic fraction will be even lower by an overall scale factor as compared to the one shown in Fig. 4(c). We note the nonmonotonous temperature dependence of the magnetic fraction for $Ba_{0.35}Rb_{0.65}Fe_2As_2$. This kind of T dependence of V_m was previously observed in a number of Fe-HTS's [63,64] with the static magnetism and may be caused by the interplay between magnetism and superconductivity.

The TF μSR data were analyzed by using the following functional form [51,60,65]:

$$A_{TF_S}(t) = A_S e^{-\Lambda_{TF} t} e^{[-\frac{(\sigma_{sc}^2 + \sigma_{nm}^2)t^2}{2}]} \cos(\gamma_\mu B_{\rm int} t + \varphi), \quad (2)$$

Here A denotes the initial asymmetry, $\gamma/(2\pi) \simeq 135.5$ MHz/T is the muon gyromagnetic ratio, and φ is the initial phase of the muon-spin ensemble. Λ is the exponential relaxation rate caused by the presence of diluted Fe moments. $B_{\rm int}$ represents the internal magnetic field at the muon site, and the relaxation rates σ_{sc} and σ_{nm} characterize the damping due to the formation of the flux-line lattice (FLL) in the SC state and of the nuclear magnetic dipolar contribution, respectively. During the analysis σ_{nm} was assumed to be constant over the entire temperature range and was fixed to the value obtained above T_c where only nuclear magnetic moments contribute to the muon depolarization rate σ. Note that Eq. (2) has been used previously for Fe-HTS's in the presence of the diluted Fe moments, and it was demonstrated to be precise enough to extract the SC depolarization rate as a function of temperature [60]. The temperature dependence of the difference between the internal field $\mu_0 H_{\rm int,SC}$ measured in SC state and one $\mu_0 H_{\rm int,NS}$ measured in the normal state at $T = 45$ K for $Ba_{1-x}Rb_xFe_2As_2$ ($x = 0.35$ and 0.65) is shown in Fig. 5(a), revealing a strong diamagnetic shift imposed by the SC state. In Fig. 5(b) σ_{sc} is plotted as a function of temperature for $Ba_{1-x}Rb_xFe_2As_2$ ($x = 0.35$ and 0.65) at $\mu_0 H = 0.05$ T. Below T_c the relaxation rate σ_{sc} starts to increase from zero due to the formation of the FLL. The value of σ_{sc} is lower for the over-doped sample than the one of the optimally-doped system. In addition, an interesting experimental fact is that the T dependence of the relaxation rate, which reflects the topology of the SC gap, changes between $x = 0.35$ and 0.65. The data for $x = 0.35$ is flat below $T/T_c \simeq 0.4$, indicating a fully gapped SC state. In contrast, the data for $x = 0.65$ exhibits a steeper temperature dependence of $\sigma_{sc}(T)$, indicating the presence of quasiparticle excitations. In order to quantify the change of the symmetry of the SC gap, we analyzed the T dependence of the magnetic penetration depth. For polycrystalline samples the temperature dependence of

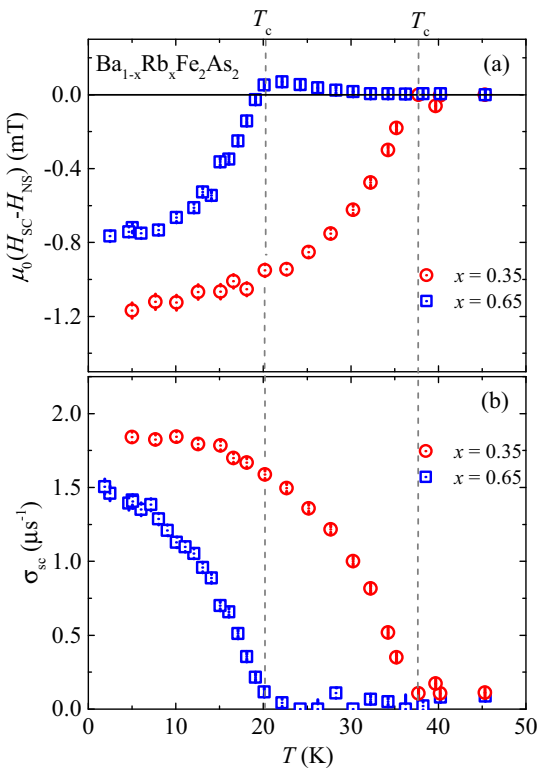

FIG. 5. (a) Temperature dependence of the difference between the internal field $\mu_0 H_{SC}$ measured in the SC state and the one measured in the normal state $\mu_0 H_{NS}$ at $T = 50$ K for $Ba_{1-x}Rb_xFe_2As_2$ ($x = 0.35$ and 0.65). (b) Temperature dependence of the superconducting muon spin depolarization rate σ_{sc} measured in an applied magnetic field of $\mu_0 H = 0.05$ T for both samples.

the London magnetic penetration depth $\lambda(T)$ is related to the muon spin depolarization rate $\sigma_{sc}(T)$ by the equation [66]:

$$\frac{\sigma_{sc}^2(T)}{\gamma_\mu^2} = 0.00371\frac{\Phi_0^2}{\lambda^4(T)}, \tag{3}$$

where $\Phi_0 = 2.068\times10^{-15}$ Wb is the magnetic-flux quantum. Equation (2) is only valid when the separation between the vortices is smaller than λ. In this case, according to the London model, σ_{sc} is field independent [66]. Field dependent measurements of σ_{sc} for the $x = 0.35$ sample were reported previously [11]. It was observed that first σ_{sc} strongly increases with increasing magnetic field until reaching a maximum at $\mu_0 H \simeq 0.03$ T and then above 0.03 T stays nearly constant up to the highest field (0.64 T) investigated. Such a behavior is expected within the London model and is typical for polycrystalline high temperature superconductors (HTS's) [67]. The observed field dependence of σ_{sc} implies that for a reliable determination of the penetration depth the applied field must be larger than $\mu_0 H = 0.03$ T.

$\lambda(T)$ can be calculated within the local (London) approximation ($\lambda \gg \xi$) by the following expression [51,68]:

$$\frac{\lambda^{-2}(T,\Delta_{0,i})}{\lambda^{-2}(0,\Delta_{0,i})} = 1 + \frac{1}{\pi}\int_0^{2\pi}\int_{\Delta(T,\varphi)}^{\infty}\left(\frac{\partial f}{\partial E}\right)\frac{E\,dE\,d\varphi}{\sqrt{E^2-\Delta_i(T,\varphi)^2}}, \tag{4}$$

where $f = [1+\exp(E/k_BT)]^{-1}$ is the Fermi function, φ is the angle along the Fermi surface, and $\Delta_i(T,\varphi) = \Delta_{0,i}\Gamma(T/T_c)g(\varphi)$ ($\Delta_{0,i}$ is the maximum gap value at $T = 0$). The temperature dependence of the gap is approximated by the expression $\Gamma(T/T_c) = \tanh\{1.82[1.018(T_c/T-1)]^{0.51}\}$ [69], while $g(\varphi)$ describes the angular dependence of the gap, and it is replaced by 1 for both an s-wave and an s+s-wave gap, and $|\cos(2\varphi)|$ for a d-wave gap [70].

The temperature dependence of the penetration depth was analyzed using either a single gap or a two-gap model which is based on the so-called α model. This model was first discussed by Padamsee *et al.* [71] and later on was successfully used to analyze the magnetic penetration depth data in HTS's [69,72]. According to the α model, the superfluid density is calculated for each component using Eq. (3) and then the contributions from the two components added together, i.e.,

$$\frac{\lambda^{-2}(T)}{\lambda^{-2}(0)} = \omega_1\frac{\lambda^{-2}(T,\Delta_{0,1})}{\lambda^{-2}(0,\Delta_{0,1})} + \omega_2\frac{\lambda^{-2}(T,\Delta_{0,2})}{\lambda^{-2}(0,\Delta_{0,2})}, \tag{5}$$

where $\lambda^{-2}(0)$ is the penetration depth at zero temperature, $\Delta_{0,i}$ is the value of the ith ($i = 1, 2$) superconducting gap at $T = 0$ K, and ω_i is a weighting factor which measures their relative contributions to λ^{-2} ($\omega_1 + \omega_2 = 1$).

The results of the analysis for $Ba_{1-x}Rb_xFe_2As_2$ ($x = 0.35$, 0.65) are presented in Fig. 6. The lines represent fits to the data using a s-wave model (dashed line) and $s+s$-wave and d-wave models (solid lines). In agreement with our previous report [11] the two-gap s+s-wave scenario with a small gap $\Delta_1 = 2.7(5)$ meV and a large gap $\Delta_2 = 8.41(23)$ meV, describes the experimental data for the optimally doped $x = 0.35$ sample fairly well. On the other hand, for the over-doped sample $x = 0.65$ a d-wave gap symmetry with a gap $\Delta = 8.2(7)$ meV gives an adequate description of $\lambda^{-2}(T)$. This conclusion is supported by a χ^2 test, revealing the smaller value of χ^2 for d-wave model by ~25% than the one for $s+s$-wave model. Furthermore, we note that the $s+s$-wave model fit gives the following value for the smaller

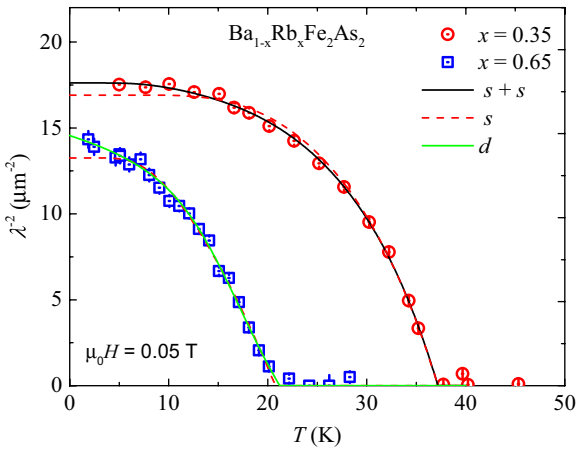

FIG. 6. The temperature dependence of λ^{-2} for $Ba_{1-x}Rb_xFe_2As_2$ ($x = 0.35$, 0.65), measured in an applied field of $\mu_0 H = 0.05$ T. The dashed lines correspond to a single gap BCS s-wave model, whereas the solid ones represent fits using a two-gap ($s+s$)-wave and a d-wave model.

gap $\Delta_1 = 0.6(5)$ meV which is comparable to zero, ruling out this model as a possible description of $\lambda(T)$ for the over-doped sample $x = 0.65$. This suggests that the heavy hole-doping in $Ba_{1-x}Rb_xFe_2As_2$ induces a change of the SC gap topology from nodeless to nodal, as it is the case for the related system $Ba_{1-x}K_xFe_2As_2$.

2. *High pressure zero-field and transverse-field μSR experiments on* $Ba_{0.35}Rb_{0.65}Fe_2As_2$

Figure 7(a) shows the ZF-μSR time spectra for $p = 0$ and 2.3 GPa obtained at $T = 2.5$ K for $Ba_{0.35}Rb_{0.65}Fe_2As_2$. The ZF relaxation rate stays nearly unchanged between $p = 0$ GPa and 2.3 GPa, implying that there is no sign of pressure induced magnetism in this system. Figures 7(b) and 7(c) exhibit the TF time spectra for $Ba_{0.65}Rb_{0.35}Fe_2As_2$, measured at ambient $p = 0$ GPa and maximum applied pressure $p = 2.3$ GPa, respectively. Spectra above (45 K) and below (1.7 K) the SC transition temperature T_c are shown. The TF μSR data were

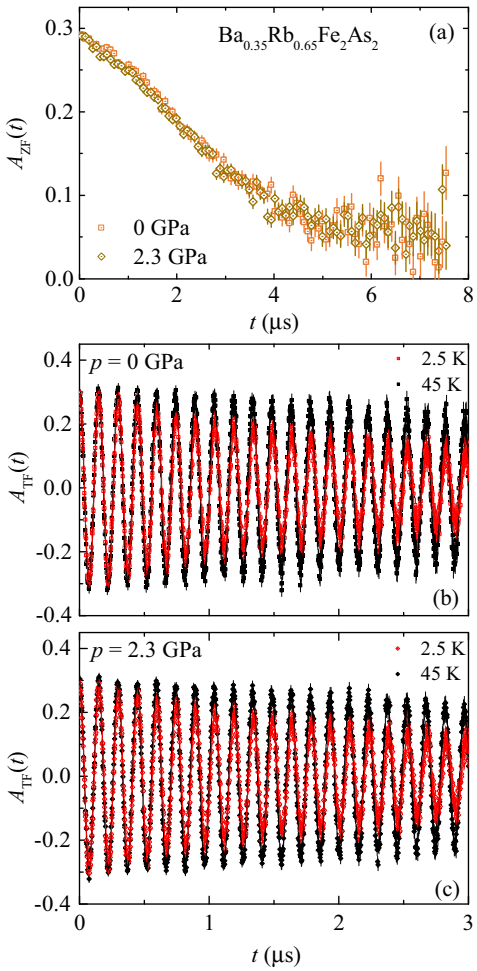

FIG. 7. (a) ZF-μSR time spectra for $Ba_{0.35}Rb_{0.65}Fe_2As_2$ for $p = 0$ and 2.3 GPa at the base temperature $T = 2.5$ K. Transverse-field (TF) μSR time spectra obtained above and below T_c for $Ba_{0.35}Rb_{0.65}Fe_2As_2$ (after field cooling the sample from above T_c): (b) $p = 0$ GPa and (c) $p = 2.3$ GPa. The solid lines in panel (b) and (c) represent fits to the data by means of Eq. (6).

analyzed by using the following functional form [51]:

$$A_{\rm TF}(t) = A_{TF_s}(t) + A_{\rm pc}\exp\left[-\frac{\sigma_{\rm pc}^2 t^2}{2}\right]\cos(\gamma_\mu B_{\rm int,pc}t + \varphi). \quad (6)$$

Here $P_s(t)$ is the function used to describe the sample response and is given by Eq. (2). $A_{\rm pc}$ denote the initial asymmetry of the pressure cell. φ is the initial phase of the muon-spin ensemble and $B_{\rm int,pc}$ represents the internal magnetic field probed by the muons, stopped in the pressure cell. The Gaussian relaxation rate $\sigma_{\rm pc}$ reflects the depolarization due to the nuclear magnetism of the pressure cell. As shown previously [73], the diamagnetism of the SC sample has an influence on the pressure cell signal, leading to the temperature dependent $\sigma_{\rm pc}$ below T_c. In order to consider the influence of the diamagnetic moment of the sample on the pressure cell [73], we assume the linear coupling between $\sigma_{\rm pc}$ and the field shift of the internal magnetic field in the SC state: $\sigma_{\rm pc}(T) = \sigma_{\rm pc}(T > T_c) + c(T)(\mu_0 H_{\rm int,NS} - \mu_0 H_{\rm int,SC})$, where $\sigma_{\rm pc}(T > T_c) = 0.35\ \mu s^{-1}$ is the temperature independent Gaussian relaxation rate. $\mu_0 H_{\rm int,NS}$ and $\mu_0 H_{\rm int,SC}$ are the internal magnetic fields measured in the normal and in the SC state, respectively. As indicated by the solid lines in Figs. 7(b) and 7(c), the μSR data are well described by Eq. (6).

A large diamagnetic shift of $\mu_0 H_{\rm int}$ sensed by the muons below T_c is observed at all applied pressures. This is evident in Fig. 8(a), where we plot the difference between the internal field $\mu_0 H_{\rm int,SC}$ measured in SC state and $\mu_0 H_{\rm int,NS}$ measured in the normal state at $T = 45$ K for $Ba_{0.35}Rb_{0.65}Fe_2As_2$. The SC transition temperature T_c is determined from the intercept of the linearly extrapolated $\mu_0(H_{\rm int,SC} - H_{\rm int,NS})$ curve with its zero line, and it is found to be $T_c = 21.6(7)$ K and 19.2(5) for $p = 0$ GPa and 2.3 GPa, respectively. The ambient pressure value of T_c is in perfect agreement with the one $T_c = 20.9(5)$ K obtained from magnetization and specific heat experiments. With the highest pressure applied $p = 2.3$ GPa T_c decreases by $\sim$2.4 K, corresponding to a stronger pressure effect on T_c as compared to the one observed in the optimally doped sample $Ba_{0.65}Rb_{0.35}Fe_2As_2$. The temperature dependence of $\sigma_{\rm sc}$ for $Ba_{0.35}Rb_{0.65}Fe_2As_2$ at various pressures is shown in Fig. 8(b). The inset shows the data recorded at $p = 0$ GPa for the sample measured together with the cell and without the cell. The temperature dependences as well as the relaxation rates are in good agreement with each other. While the overlap of the low-T data for $p = 0$, 0.54 and 1.02 GPa is observed, it is clear that $\sigma_{\rm sc}$ for the highest applied pressure $p = 2.3$ GPa has slightly steeper T dependence at low temperatures. This leads to a tiny pressure induced decrease of the zero-temperature value of the penetration depth $\lambda(0)$, which is different from the observation for the $x = 0.35$ sample where a substantial decrease of $\lambda(0)$ was reported. Note that for all applied pressures the temperature dependence of λ^{-2} is well described by a d-wave gap symmetry as shown in Fig. 9. This implies that the d-wave symmetry in over-doped $Ba_{0.35}Rb_{0.65}Fe_2As_2$ is robust against pressure. The results of the $x = 0.65$ sample extracted from the analysis of the pressure data are summarized in Table I. We note that the nodal SC gaps are promoted in the optimally doped $x = 0.35$ system under pressure, as shown in our previous work [11]. However, the nodes exist only on the

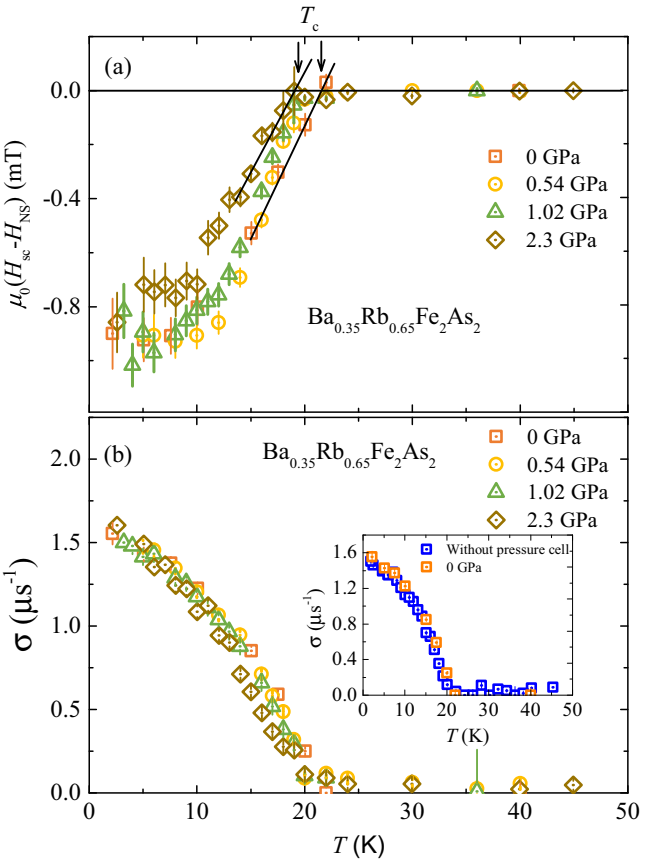

FIG. 8. (a) Temperature dependence of the difference between the internal field $\mu_0 H_{SC}$ measured in the SC state and the one measured in the normal state $\mu_0 H_{NS}$ at $T = 45$ K for $Ba_{0.65}Rb_{0.35}Fe_2As_2$ recorded for various hydrostatic pressures. (b) Temperature dependence of the superconducting muon spin depolarization rate σ_{sc} in an applied magnetic field of $\mu_0 H = 50$ mT for $Ba_{0.35}Rb_{0.65}Fe_2As_2$ for selected applied pressures. The inset shows the data recorded at $p = 0$ GPa for the sample measured together with the cell and without the cell.

hole pockets, while the electron pockets have nearly uniform gaps. But in case of the over-doped $x = 0.65$ system, the results are consistent with the presence of nodal d-wave gaps on all Fermi surface sheets. It is important to emphasize that

TABLE I. Summary of the parameters obtained for polycrystalline samples of $Ba_{0.35}Rb_{0.65}Fe_2As_2$ by means of μSR.

p (GPa)	T_c (K)	Δ (meV)	$2\Delta/k_BT_c$	λ (nm)
0	22.44(13)	8.2(7)	8.55(47)	257(5)
0.54	21.97(15)	6.4(3)	6.83(47)	254(5)
1.02	21.32(18)	6.3(3)	6.88(59)	256(6)
2.3	19.8(2)	5.3(3)	6.1(6)	250(6)

by heavy hole doping as well as hydrostatic pressure, one can induce stable d-wave pairing in $Ba_{1-x}Rb_xFe_2As_2$. The recent theoretical and experimental [49] studies of optimally-doped $Ba_{0.6}K_{0.4}Fe_2As_2$ revealed a subdominant d-wave state close in energy to an s^{+-} state. It was shown that the coupling strength in this subdominant d channel is as strong as 60% of that in the dominant s^{+-} channel. According to the results, presented and discussed above, pressure and heavy hole doping tip the intricate balance between d and s in favor of a d-wave state.

IV. PHASE DIAGRAM

The results of $\lambda^{-2}(T)$ for $Ba_{0.35}Rb_{0.65}Fe_2As_2$ analysis are summarized in Figs. 10(a)–10(d), showing T_c as well as the zero-temperature values of $\lambda(0)$, the SC d-wave gap Δ, and the gap to T_c ratio $2\Delta/k_BT_c$ as a function of hydrostatic pressure. Upon increasing the hydrostatic pressure from $p = 0$ to 2.3 GPa, $\lambda(0)$ is increased by less than 5% and T_c is decreased by 10%. Both Δ and $2\Delta/k_BT_c$ shows only a modest decrease with increasing pressure. Our results show that there are no significant changes of the SC properties of $Ba_{0.35}Rb_{0.65}Fe_2As_2$ under pressure and d represents the most stable pairing symmetry in $Ba_{0.35}Rb_{0.65}Fe_2As_2$. In order to reach a more complete view of the pressure effect on $\sigma_{sc}(0)$ and T_c in $Ba_{1-x}Rb_xFe_2As_2$ in Figs. 10(a) and 10(b) we combined the present data with the previous high-pressure μSR results on optimally doped $Ba_{0.65}Rb_{0.35}Fe_2As_2$ and on $RbFe_2As_2$ which presents the case of a naturally over-doped system. For all samples, the $T_c(p)$ and $\lambda(0)(p)$ behaviors are linear, so that the pressure dependence of T_c and $\lambda(0)$ can be well represented by dT_c/dp and $d\lambda(0)/dp$ values, respectively. The pressure derivative, dT_c/dp, is negative for all $x = 0.35$, 0.65, 1 and its magnitude increases with increasing x. However, there is

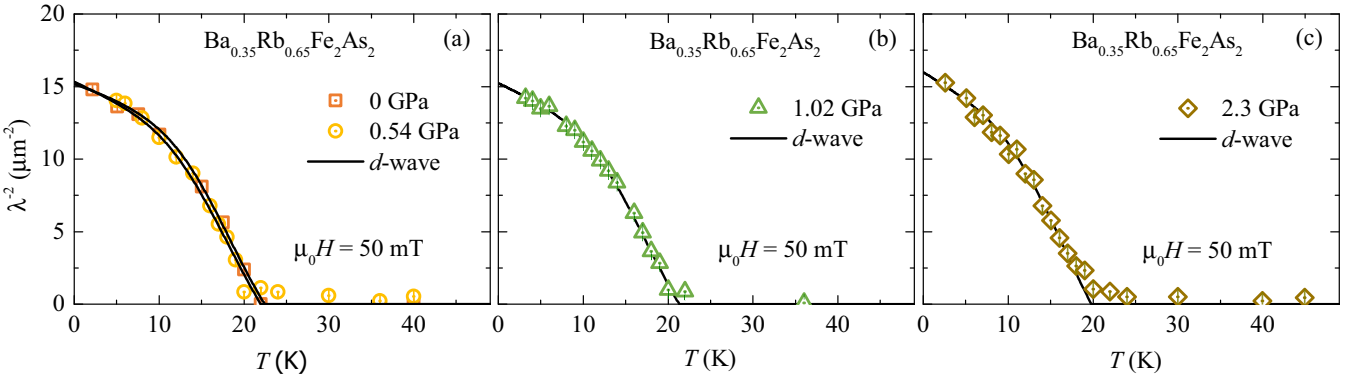

FIG. 9. (a-c) The temperature dependence of λ^{-2} measured at various applied hydrostatic pressures for $Ba_{0.35}Rb_{0.65}Fe_2As_2$ in an applied field of $\mu_0 H = 50$ mT. The solid lines correspond to a single-gap d-wave model.

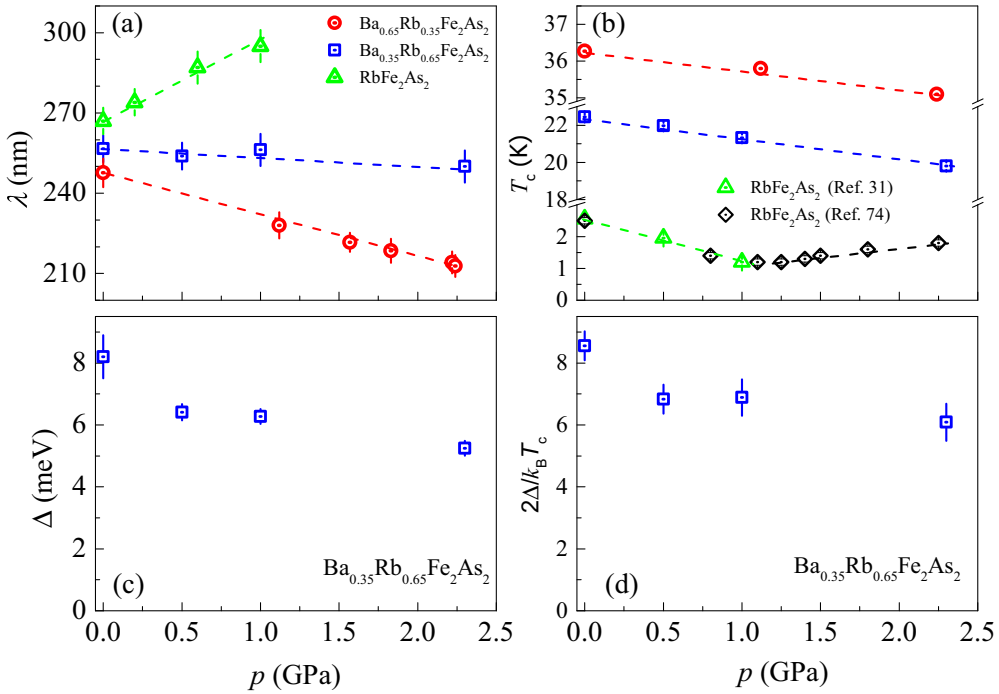

FIG. 10. The zero temperature value of the magnetic penetration depth $\lambda(0)$ (a) and the SC transition temperature T_c (b) for $Ba_{1-x}Rb_xFe_2As_2$ ($x = 0.35$, 0.65, 1.0), as well as the d-wave gap (c) and the gap to T_c ratio $2\Delta/k_BT_c$ (d) for the over-doped sample $x = 0.65$, plotted as a function of hydrostatic pressure. The measurements were performed in an applied magnetic field of $\mu_0 H = 50$ mT. The data for $x = 0.35$ sample are taken from Ref. [39], and the data for $x = 1$ are taken from Refs. [31] and [74]. The dashed lines represent the guides to the eyes.

at higher pressures a fundamental difference of $T_c(p)$ between the $x = 0.35$, 0.65 and $x = 1$ samples. Namely, for $x = 1$ a V-shaped temperature pressure phase diagram is observed [74] as in KFe_2As_2 [38] which is absent for $x = 0.35$ and 0.65 up to the highest applied pressure of $p = 2.3$ GPa. Regarding $\lambda(0)$, application of pressure of $p = 2.3$ GPa causes a decrease of its value by 15% in optimally doped sample $x = 0.35$, while only a very tiny decrease of $\lambda(0)$ is observed for the over-doped system $x = 0.65$. Instead, for the end member compound an increase of $\lambda(0)$ with pressure is observed. This means that the $d\lambda(0)/dp$ is negative and large for $x = 0.35$. On further increasing the x to 0.65 it's magnitude becomes negligibly small but is still negative and becomes positive for the end member $x = 1$. So, the sign change of $d\lambda(0)/dp$ takes place for some of the x values located between $x = 0.65$ and 1. The above results provide clear evidence that the SC gap symmetry as well as the pressure effects on T_c and on $\lambda(0)$ strongly depend on doping level x. Note that in the optimally doped '122'-system $Ba_{1-x}K_xFe_2As_2$ several bands cross the Fermi surface (FS) [9,75,76]. They consist of inner (α) and outer (β) holelike bands, both centered at the zone center Γ, and an electronlike band (γ) centered at the M point. Band structure of $Ba_{1-x}K_xFe_2As_2$ changes are associated with hole doping. The hole Fermi surfaces expand with increasing x, whereas electron Fermi surfaces shrink gradually and disappear for $x >$ 0.6, giving rise to a Lifshitz transition. Since, the investigated system is very similar to $Ba_{1-x}K_xFe_2As_2$, one expects similar doping induced changes in the band structure in both materials. Hence, the x dependence of the SC gap symmetry as well as the pressure effects, reported above for $Ba_{1-x}Rb_xFe_2As_2$, may be related to this putative Lifshitz transition.

V. SUMMARY AND CONCLUSIONS

In summary, the SC properties of optimally and over-doped $Ba_{1-x}Rb_xFe_2As_2$ ($x = 0.35$ and 0.65) samples at ambient pressure were studied by means of magnetization, specific heat, and μSR experiments. In addition, the $x = 0.65$ specimen was investigated under hydrostatic pressures up to $p = 2.3$ GPa through zero-field and transverse field μSR experiments. While the specific heat jump for the $x = 0.35$ sample follows the so-called BNC scaling, the heavily over-doped $Ba_{1-x}Rb_xFe_2As_2$ shows a deviation from the BNC scaling as it was observed for the related $Ba_{1-x}K_xFe_2As_2$ system. In contrast to nodeless SC gap observed in the optimally doped sample $x = 0.35$, the temperature dependence of the magnetic penetration depth λ suggests a d-wave SC gap in over-doped system $x = 0.65$. The d-wave symmetry is preserved under hydrostatic pressures up to $p = 2.3$ GPa, indicating the robustness of the d-wave symmetry in the over-doped region. The fact that the rather stable d-wave symmetry was also observed in the optimally-doped sample $x = 0.35$ under pressure indicates that both tuning parameters, heavy hole doping and hydrostatic pressure, promote the same pairing symmetry for superconductivity in $Ba_{1-x}Rb_xFe_2As_2$. The values of the magnetic penetration depth λ, T_c as well as the d-wave gap Δ and the ratio $2\Delta/k_BT_c$ show a small and monotonic decrease with increasing the pressure. By combining the present data with those previously obtained for the optimally doped system [39] and for the end member $RbFe_2As_2$ [31] we conclude that the SC gap symmetry as well as the pressure effects on the quantities characterizing the SC state strongly depends on the hole doping level x. The combined results may

be interpreted by assuming a disappearance of the electron pocket from the Fermi surface upon the high hole doping, resulting in a Lifshitz transition. Note that the absence of the γ electron pocket has been observed by ARPES in the related system KFe_2As_2 [29]. Finally, we suggest that the $Ba_{1-x}Rb_xFe_2As_2$ and $Ba_{1-x}K_xFe_2As_2$ superconducting series have a common doping dependence of the SC properties. The present results may help to explore the microscopic mechanism responsible for the observed nonuniversality of the SC gap structure in the Fe-HTS's.

ACKNOWLEDGMENTS

The work was performed at the Swiss Muon Source ($S\mu S$) Paul Scherrer Insitute, Villigen, Switzerland. Z.G. gratefully acknowledges the financial support by the Swiss National Science Foundation (SNF Grant No. 200021-149486).

[1] J. G. Bednorz and K. A. Müller, Z. Phys. B **64**, 189 (1986).
[2] F. Steglich, J. Aarts, C. D. Bredl, W. Lieke, D. Meschede, W. Franz, and H. Schäfer, Phys. Rev. Lett. **43**, 1892 (1979).
[3] D. Jerome, A. Mazaud, M. Ribault, and K. Bechgaard, J. Phys. Lett. **41**, 95 (1980).
[4] Y. Kamihara, T. Watanabe, M. Hirano, and H. Hosono, J. Am. Chem. Soc. **130**, 3296 (2008).
[5] H. Takahashi, K. Igawa, K. Arii, Y. Kamihara, M. Hirano, and H. Hosono, Nature (London) **453**, 376 (2008).
[6] Y. J. Uemura, Nat. Mater. **8**, 253 (2009).
[7] C. W. Chu, Nat. Phys. **5**, 787 (2009).
[8] G. Zhao, Phys. Scr. **83**, 038302 (2011).
[9] H. Ding, P. Richard, K. Nakayama, T. Sugawara, T. Arakane, Y. Sekiba, A. Takayama, S. Souma, T. Sato, T. Takahashi, Z. Wang, X. Dai, Z. Fang, G. F. Chen, J. L. Luo, and N. L. Wang, Europhys. Lett. **83**, 47001 (2008).
[10] R. Khasanov, D. V. Evtushinsky, A. Amato, H.-H. Klauss, H. Luetkens, Ch. Niedermayer, B. Büchner, G. L. Sun, C. T. Lin, J. T. Park, D. S. Inosov, and V. Hinkov, Phys. Rev. Lett. **102**, 187005 (2009).
[11] Z. Guguchia, Z. Shermadini, A. Amato, A. Maisuradze, A. Shengelaya, Z. Bukowski, H. Luetkens, R. Khasanov, J. Karpinski, and H. Keller, Phys. Rev. B **84**, 094513 (2011).
[12] K. Terashima, Y. Sekiba, J. H. Bowen, K. Nakayama, T. Kawahara, T. Sato, P. Richard, Y.-M. Xu, L. J. Li, G. H. Cao, Z.-A. Xu, H. Ding, and T. Takahashi, Proc. Natl. Acad. Sci. USA **106**, 7330 (2009).
[13] Y. Zhang, L. X. Yang, M. Xu, Z. R. Ye, F. Chen, C. He, H. C. Xu, J. Jiang, B. P. Xie, J. J. Ying, X. F. Wang, X. H. Chen, J. P. Hu, M. Matsunami, S. Kimura, and D. L. Feng, Nat. Mater. **10**, 273 (2011).
[14] H. Miao, P. Richard, Y. Tanaka, K. Nakayama, T. Qian, K. Umezawa, T. Sato, Y.-M. Xu, Y.-B. Shi, N. Xu, X.-P. Wang, P. Zhang, H.-B. Yang, Z.-J. Xu, J. S. Wen, G.-D. Gu, X. Dai, J.-P. Hu, T. Takahashi, and H. Ding, Phys. Rev. B **85**, 094506 (2012).
[15] Mahmoud Abdel-Hafiez, Zheng He, Jun Zhao, Xingye Lu, Huiqian Luo, Pengcheng Dai, and Xiao-Jia Chen, arXiv:1502.07130.
[16] P. K. Biswas, G. Balakrishnan, D. M. Paul, C. V. Tomy, M. R. Lees, and A. D. Hillier, Phys. Rev. B **81**, 092510 (2010).
[17] J. D. Fletcher, A. Serafin, L. Malone, J. G. Analytis, J.-H. Chu, A. S. Erickson, I. R. Fisher, and A. Carrington, Phys. Rev. Lett. **102**, 147001 (2009).
[18] K. Hashimoto, M. Yamashita, S. Kasahara, Y. Senshu, N. Nakata, S. Tonegawa, K. Ikada, A. Serafin, A. Carrington, T. Terashima, H. Ikeda, T. Shibauchi, and Y. Matsuda, Phys. Rev. B **81**, 220501 (2010).
[19] M. Yamashita, Y. Senshu, T. Shibauchi, S. Kasahara, K. Hashimoto, D. Watanabe, H. Ikeda, T. Terashima, I. Vekhter, A. B. Vorontsov, and Y. Matsuda, Phys. Rev. B **84**, 060507 (2011).
[20] Yusuke Nakai, Tetsuya Iye, Shunsaku Kitagawa, Kenji Ishida, Shigeru Kasahara, Takasada Shibauchi, Yuji Matsuda, and Takahito Terashima, Phys. Rev. B **81**, 020503 (2010).
[21] K. Hashimoto, S. Kasahara, R. Katsumata, Y. Mizukami, M. Yamashita, H. Ikeda, T. Terashima, A. Carrington, Y. Matsuda, and T. Shibauchi, Phys. Rev. Lett. **108**, 047003 (2012).
[22] J. K. Dong, S. Y. Zhou, T. Y. Guan, H. Zhang, Y. F. Dai, X. Qiu, X. F. Wang, Y. He, X. H. Chen, and S. Y. Li, Phys. Rev. Lett. **104**, 087005 (2010).
[23] X. Qiu, S. Y. Zhou, H. Zhang, B. Y. Pan, X. C. Hong, Y. F. Dai, M. J. Eom, J. S. Kim, Z. R. Ye, Y. Zhang, D. L. Feng, and S. Y. Li, Phys. Rev. X **2**, 011010 (2012).
[24] Can-Li Song, Yi-Lin Wang, Peng Cheng, Ye-Ping Jiang, Wei Li, Tong Zhang, Zhi Li, Ke He, Lili Wang, Jin-Feng Jia, Hsiang-Hsuan Hung, Congjun Wu, Xucun Ma, Xi Chen, and Qi-Kun Xue, Science **332**, 1410 (2010).
[25] Y. Zhang, Z. R. Ye, Q. Q. Ge, F. Chen, Juan Jiang, M. Xu, B. P. Xie, and D. L. Feng, Nat. Phys. **8**, 371 (2012).
[26] Simon Peschke, Tobias Stürzer, and Dirk Johrendt, J. Inorg. Gen. Chem. **640**, 830 (2014).
[27] J.-Ph. Reid, A. Juneau-Fecteau, R. T. Gordon, S. Rene de Cotret, N. Doiron-Leyraud, X. G. Luo, H. Shakeripour, J. Chang, M. A. Tanatar, H. Kim, R. Prozorov, T. Saito, H. Fukazawa, Y. Kohori, K. Kihou, C. H. Lee, A. Iyo, H. Eisaki, B. Shen, H.-H. Wen, and Louis Taillefer, Supercond. Sci. Technol. **25**, 084013 (2012).
[28] Masanori Hirano, Yuji Yamada, Taku Saito, Ryo Nagashima, Takehisa Konishi, Tatsuya Toriyama, Yukinori Ohta, Hideto Fukazawa, Yoh Kohori, Yuji Furukawa, Kunihiro Kihou, Chul-Ho Lee, Akira Iyo, and Hiroshi Eisaki, J. Phys. Soc. Jpn. **81**, 054704 (2012).
[29] T. Sato, K. Nakayama, Y. Sekiba, P. Richard, Y.-M. Xu, S. Souma, T. Takahashi, G. F. Chen, J. L. Luo, N. L. Wang, and H. Ding, Phys. Rev. Lett. **103**, 047002 (2009).
[30] Z. Shermadini, J. Kanter, C. Baines, M. Bendele, Z. Bukowski, R. Khasanov, H.-H. Klauss, H. Luetkens, H. Maeter, G. Pascua, B. Batlogg, and A. Amato, Phys. Rev. B **82**, 144527 (2010).
[31] Z. Shermadini, H. Luetkens, A. Maisuradze, R. Khasanov, Z. Bukowski, H.-H. Klauss, and A. Amato, Phys. Rev. B **86**, 174516 (2012).
[32] Z. Zhang, A. F. Wang, X. C. Hong, J. Zhang, B. Y. Pan, J. Pan, Y. Xu, X. G. Luo, X. H. Chen, and S. Y. Li, Phys. Rev. B **91**, 024502 (2015).

[33] A. F. Wang, B. Y. Pan, X. G. Luo, F. Chen, Y. J. Yan, J. J. Ying, G. J. Ye, P. Cheng, X. C. Hong, S. Y. Li, and X. H. Chen, Phys. Rev. B **87**, 214509 (2013).

[34] X. C. Hong, X. L. Li, B. Y. Pan, L. P. He, A. F. Wang, X. G. Luo, X. H. Chen, and S. Y. Li, Phys. Rev. B **87**, 144502 (2013).

[35] H. H. Klauss, D. Baabe, D. Mienert, H. Luetkens, F. J. Litterst, B. Bchner, M. Hcker, D. Andreica, U. Zimmermann, and A. Amato, Physica B **326**, 325 (2003).

[36] R. Khasanov, S. Sanna, G. Prando, Z. Shermadini, M. Bendele, A. Amato, P. Carretta, R. De Renzi, J. Karpinski, S. Katrych, H. Luetkens, and N. D. Zhigadlo, Phys. Rev. B **84**, 100501(R) (2011).

[37] Z. Guguchia, A. Shengelaya, A. Maisuradze, L. Howald, Z. Bukowski, M. Chikovani, H. Luetkens, S. Katrych, J. Karpinski, and H. Keller, J. Supercond. Nov. Magn. **26**, 285 (2013).

[38] F. F. Tafti, A. Juneau-Fecteau, M. A. Delage, S. Cotret, J.-Ph. Reid, A. F. Wang, X.-G. Luo, X. H. Chen, N. Doiron-Leyraud, and Louis Taillefer, Nat. Phys. **9**, 349 (2013).

[39] Z. Guguchia, A. Amato, J. Kang, H. Luetkens, P. K. Biswas, G. Prando, F. von Rohr, Z. Bukowski, A. Shengelaya, H. Keller, E. Morenzoni, R. M. Fernandes, and R. Khasanov, Nat. Commun. **6**, 8863 (2015).

[40] G. Prando, T. Hartmann, W. Schottenhamel, Z. Guguchia, S. Sanna, F. Ahn, I. Nekrasov, C. G. F. Blum, A. U. B. Wolter, S. Wurmehl, R. Khasanov, I. Eremin, and B. Büchner, Phys. Rev. Lett. **114**, 247004 (2015)

[41] K. Kuroki, H. Usui, S. Onari, R. Arita, and H. Aoki, Phys. Rev. B **79**, 224511 (2009).

[42] S. Graser, A. F. Kemper, T. A. Maier, H.-P. Cheng, P. J. Hirschfeld, and D. J. Scalapino, Phys. Rev. B **81**, 214503 (2010).

[43] S. Maiti, M. M. Korshunov, T. A. Maier, P. J. Hirschfeld, and A. V. Chubukov, Phys. Rev. Lett. **107**, 147002 (2011).

[44] R. Thomale, C. Platt, W. Hanke, J. Hu, and B. A. Bernevig, Phys. Rev. Lett. **107**, 117001 (2011).

[45] M. Khodas and A. V. Chubukov, Phys. Rev. Lett. **108**, 247003 (2012).

[46] R. M. Fernandes and A. J. Millis, Phys. Rev. Lett. **110**, 117004 (2013).

[47] Jian Kang, Alexander F. Kemper, and Rafael M. Fernandes, Phys. Rev. Lett. **113**, 217001 (2014).

[48] F. Kretzschmar, B. Muschler, T. Böhm, A. Baum, R. Hackl, H.-H. Wen, V. Tsurkan, J. Deisenhofer, and A. Loidl, Phys. Rev. Lett. **110**, 187002 (2013).

[49] T. Böhm, A. F. Kemper, B. Moritz, F. Kretzschmar, B. Muschler, H.-M. Eiter, R. Hackl, T. P. Devereaux, D. J. Scalapino, and Hai-Hu Wen, Phys. Rev. X **4**, 041046 (2014).

[50] A. Maisuradze, B. Graneli, Z. Guguchia, A. Shengelaya, E. Pomjakushina, K. Conder, and H. Keller, Phys. Rev. B **87**, 054401 (2013).

[51] A. Suter and B. M. Wojek, Physics Procedia **30**, 69 (2012). The fitting of Eq. (4) was performed using the additional library BMW developped by B. Wojek.

[52] P. Walmsley, C. Putzke, L. Malone, I. Guillamón, D. Vignolles, C. Proust, S. Badoux, A. I. Coldea, M. D. Watson, S. Kasahara, Y. Mizukami, T. Shibauchi, Y. Matsuda, and A. Carrington, Phys. Rev. Lett. **110**, 257002 (2013).

[53] Sergey L. Bud'ko, Ni Ni, and Paul C. Canfield, Phys. Rev. B **79**, 220516(R) (2009).

[54] Sergey L. Bud'ko, Yong Liu, Thomas A. Lograsso, and Paul C. Canfield, Phys. Rev. B **86**, 224514 (2012).

[55] Sergey L. Bud'ko, Mihai Sturza, Duck Young Chung, Mercouri G. Kanatzidis, and Paul C. Canfield, Phys. Rev. B **87**, 100509(R) (2013).

[56] Q. Huang, Y. Qiu, W. Bao, M. A. Green, J. W. Lynn, Y. C. Gasparovic, T. Wu, G. Wu, and X. H. Chen, Phys. Rev. Lett. **101**, 257003 (2008).

[57] M. S. Torikachvili, S. L. Bud'ko, N. Ni, and P. C. Canfield, Phys. Rev. Lett. **101**, 057006 (2008).

[58] C. F. Miclea, M. Nicklas, H. S. Jeevan, D. Kasinathan, Z. Hossain, H. Rosner, P. Gegenwart, C. Geibel, and F. Steglich, Phys. Rev. B **79**, 212509 (2009).

[59] J. Zhao, Q. Huang, C. de la Cruz, S. Li, J. W. Lynn, Y. Chen, M. A. Green, G. F. Chen, G. Li, Z. Li, J. L. Luo, N. L. Wang, and P. Dai, Nat. Mater. **7**, 953 (2008).

[60] R. Khasanov, M. Bendele, A. Amato, K. Conder, H. Keller, H.-H. Klauss, H. Luetkens, and E. Pomjakushina, Phys. Rev. Lett. **104**, 087004 (2010).

[61] R. Kubo and T. Toyabe, *Magnetic Resonance and Relaxation* (North Holland, Amsterdam, 1967).

[62] R. S. Hayano, Y. J. Uemura, J. Imazato, N. Nishida, T. Yamazaki, and R. Kubo, Phys. Rev. B **20**, 850 (1979).

[63] M. Bendele, A. Amato, K. Conder, M. Elender, H. Keller, H.-H. Klauss, H. Luetkens, E. Pomjakushina, A. Raselli, and R. Khasanov, Phys. Rev. Lett. **104**, 087003 (2010).

[64] Til Goltz, Veronika Zinth, Dirk Johrendt, Helge Rosner, Gwendolyne Pascua, Hubertus Luetkens, Philipp Materne, and Hans-Henning Klauss, Phys. Rev. B **89**, 144511 (2014).

[65] Alain Yaouanc and Pierre Dalmas De Reotier, *Muon Spin Rotation, Relaxation, and Resonance* (Oxford University Press, Oxford, UK, 2010).

[66] E. H. Brandt, Phys. Rev. B **37**, 2349 (1988).

[67] B. Pümpin, H. Keller, W. Kündig, W. Odermatt, I. M. Savić, J. W. Schneider, H. Simmler, P. Zimmermann, E. Kaldis, S. Rusiecki, Y. Maeno, and C. Rossel, Phys. Rev. B **42**, 8019 (1990).

[68] M. Tinkham, *Introduction to Superconductivity* (Krieger Publishing Company, Malabar, Florida, 1975).

[69] A. Carrington and F. Manzano, Physica C **385**, 205 (2003).

[70] M. H. Fang, H. M. Pham, B. Qian, T. J. Liu, E. K. Vehstedt, Y. Liu, L. Spinu, and Z. Q. Mao, Phys. Rev. B **78**, 224503 (2008).

[71] H. Padamsee, J. E. Neighbor, and C. A. Shiffman, J. Low Temp. Phys. **12**, 387 (1973).

[72] R. Khasanov, A. Shengelaya, A. Maisuradze, F. La Mattina, A. Bussmann-Holder, H. Keller, and K. A. Müller, Phys. Rev. Lett. **98**, 057007 (2007).

[73] A. Maisuradze, A. Shengelaya, A. Amato, E. Pomjakushina, and H. Keller, Phys. Rev. B **84**, 184523 (2011).

[74] F. F. Tafti, A. Ouellet, A. Juneau-Fecteau, S. Faucher, M. Lapointe-Major, N. Doiron-Leyraud, A. F. Wang, X. G. Luo, X. H. Chen, and Louis Taillefer, Phys. Rev. B **91**, 054511 (2015).

[75] D. V. Evtushinsky, D. S. Inosov, V. B. Zabolotnyy, M. S. Viazovska, R. Khasanov, A. Amato, H.-H. Klauss, H. Luetkens, Ch. Niedermayer, G. L. Sun, V. Hinkov, C. T. Lin, A. Varykhalov, A. Koitzsch, M. Knupfer, B. Büchner, A. A. Kordyuk, and S. V. Borisenko, New J. Phys. **11**, 055069 (2009).

[76] V. B. Zabolotnyy, D. V. Evtushinsky, A. A. Kordyuk, D. S. Inosov, A. Koitzsch, A. V. Boris, G. L. Sun, C. T. Lin, M. Knupfer, B. Büchner, A. Varykhalov, R. Follath, and S. V. Borisenko, Nature (London) **457**, 569 (2009).